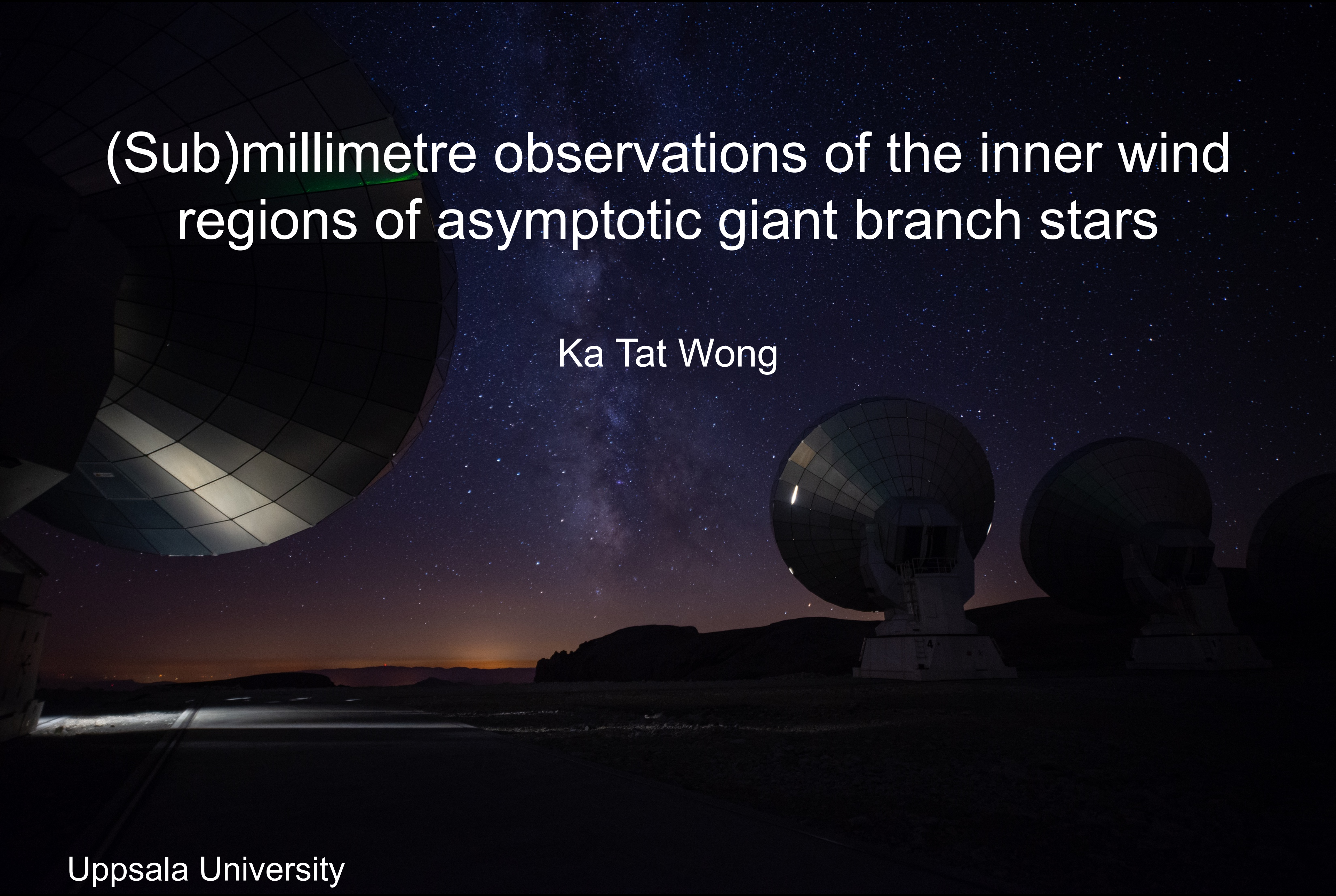

(Sub)millimetre observations of the inner wind regions of asymptotic giant branch stars

Ka Tat Wong

Uppsala University

8 September 2022

Image: © IRAM, F. Xavier Cuvelier

Life cycle of matter

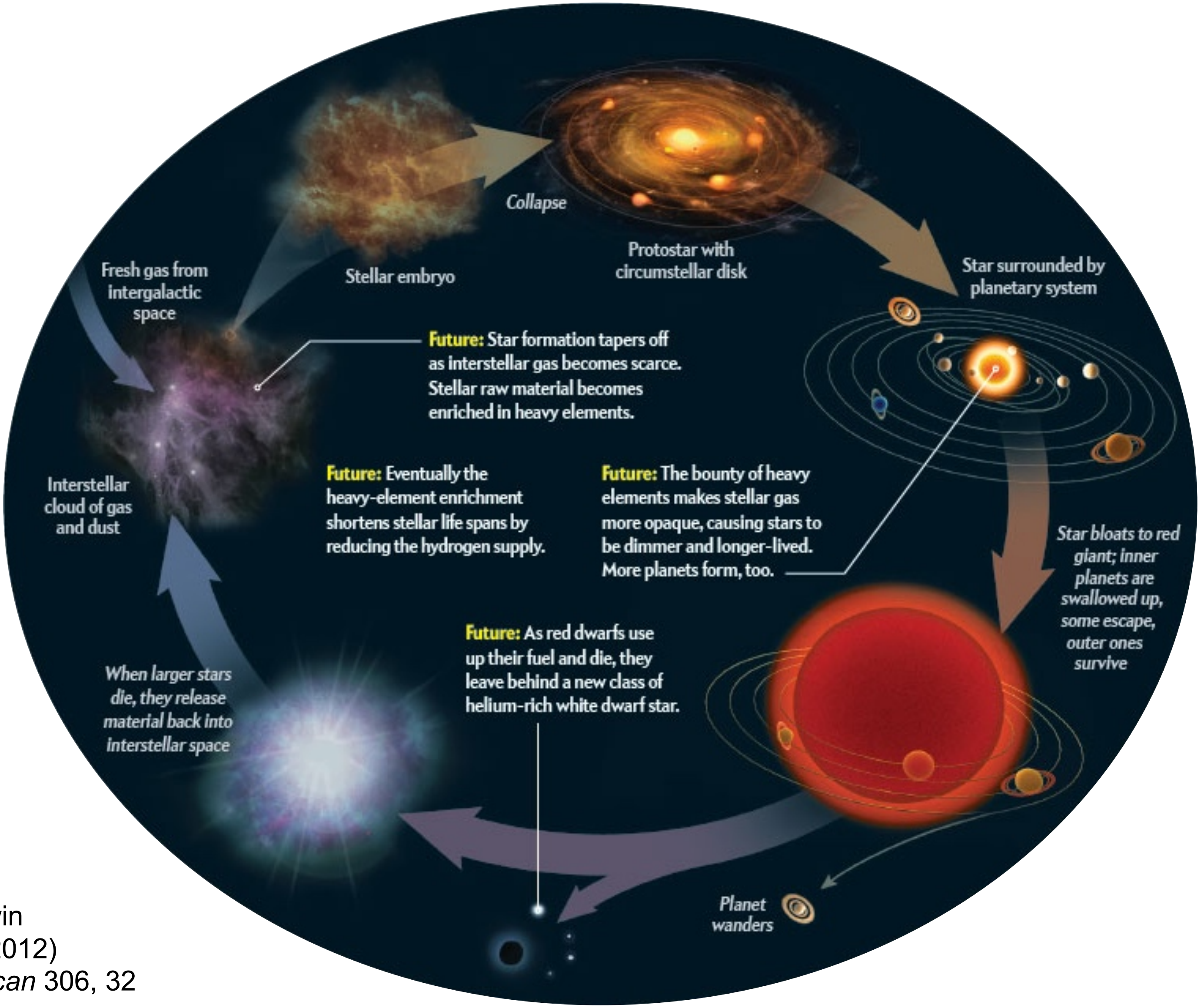

Future: Star formation tapers off as interstellar gas becomes scarce. Stellar raw material becomes enriched in heavy elements.

Future: Eventually the heavy-element enrichment shortens stellar life spans by reducing the hydrogen supply.

Future: The bounty of heavy elements makes stellar gas more opaque, causing stars to be dimmer and longer-lived. More planets form, too.

Future: As red dwarfs use up their fuel and die, they leave behind a new class of helium-rich white dwarf star.

Credit: M. Godwin
Goldsmith, D. (2012)
Scientific American 306, 32

Circumstellar envelope (CSE)

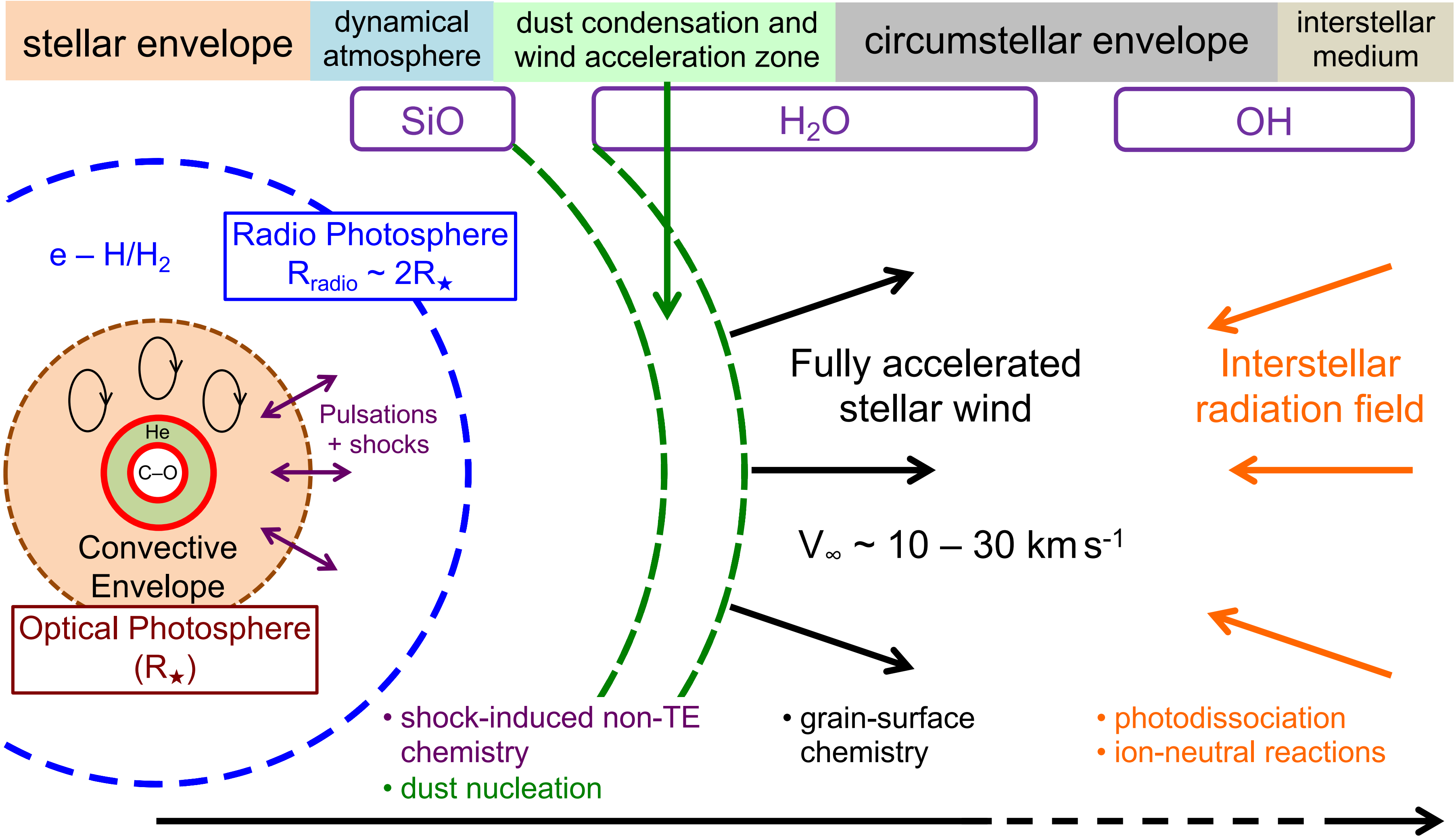

stellar envelope

dynamical atmosphere

dust condensation and wind acceleration zone

circumstellar envelope

interstellar medium

SiO

H_2O

OH

e – H/H_2

Radio Photosphere
$R_{radio} \sim 2R_\star$

He

C–O

Convective Envelope

Pulsations + shocks

Optical Photosphere
$(R_\star)$

Fully accelerated stellar wind

$V_\infty \sim 10 – 30$ km s^{-1}

Interstellar radiation field

- shock-induced non-TE chemistry
- dust nucleation

- grain-surface chemistry

- photodissociation
- ion-neutral reactions

R (AU)	0	2	4	6	8	10	Radius
T (K)		2500	1500	1000		< 500	Kinetic Temperature
n_{H_2} (cm^{-3})		10^{14}	10^{12}	10^{10}		< 10^7	Gas Density

Circumstellar chemistry

Oxygen-rich

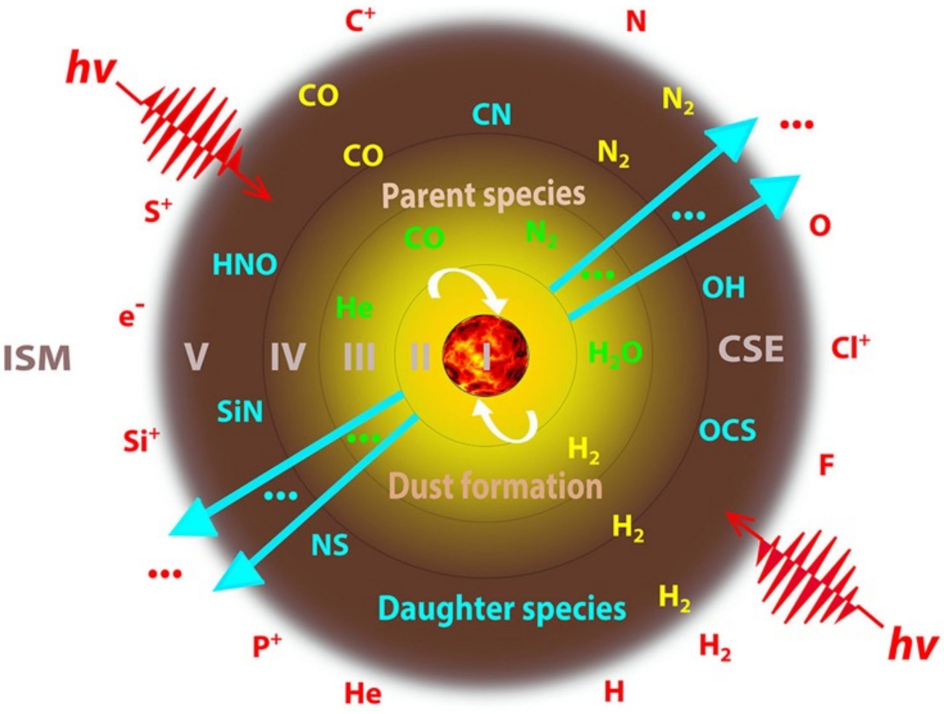

Li et al. (2016) A&A 588, A4

CO, SiO, H_2O, OH, etc.

Carbon-rich

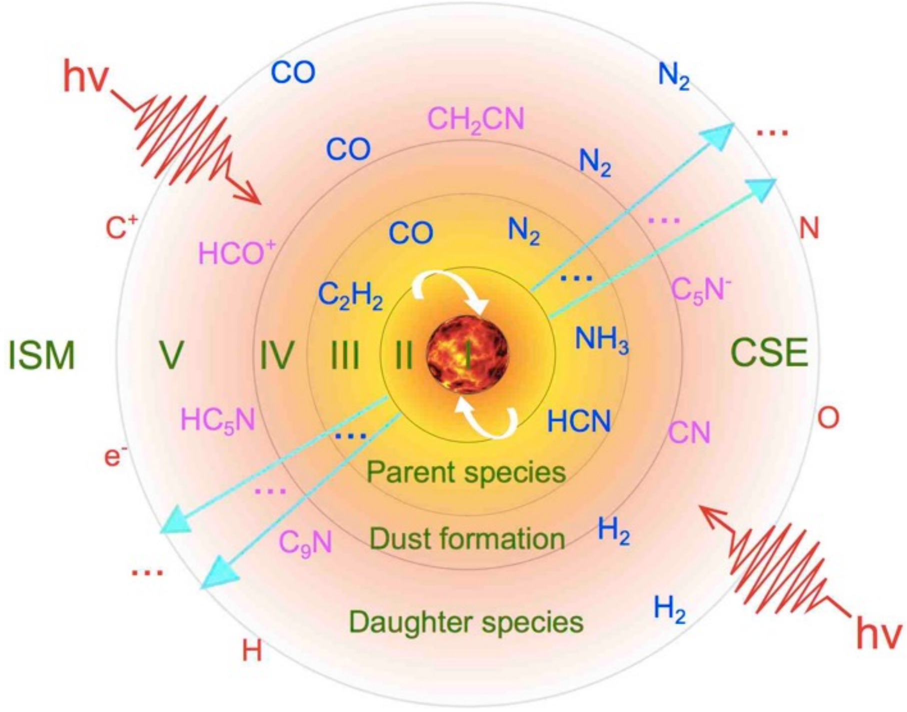

Li et al. (2014) A&A 568, A111

CO, HCN, CN, C_2H_2, etc.

Wind acceleration

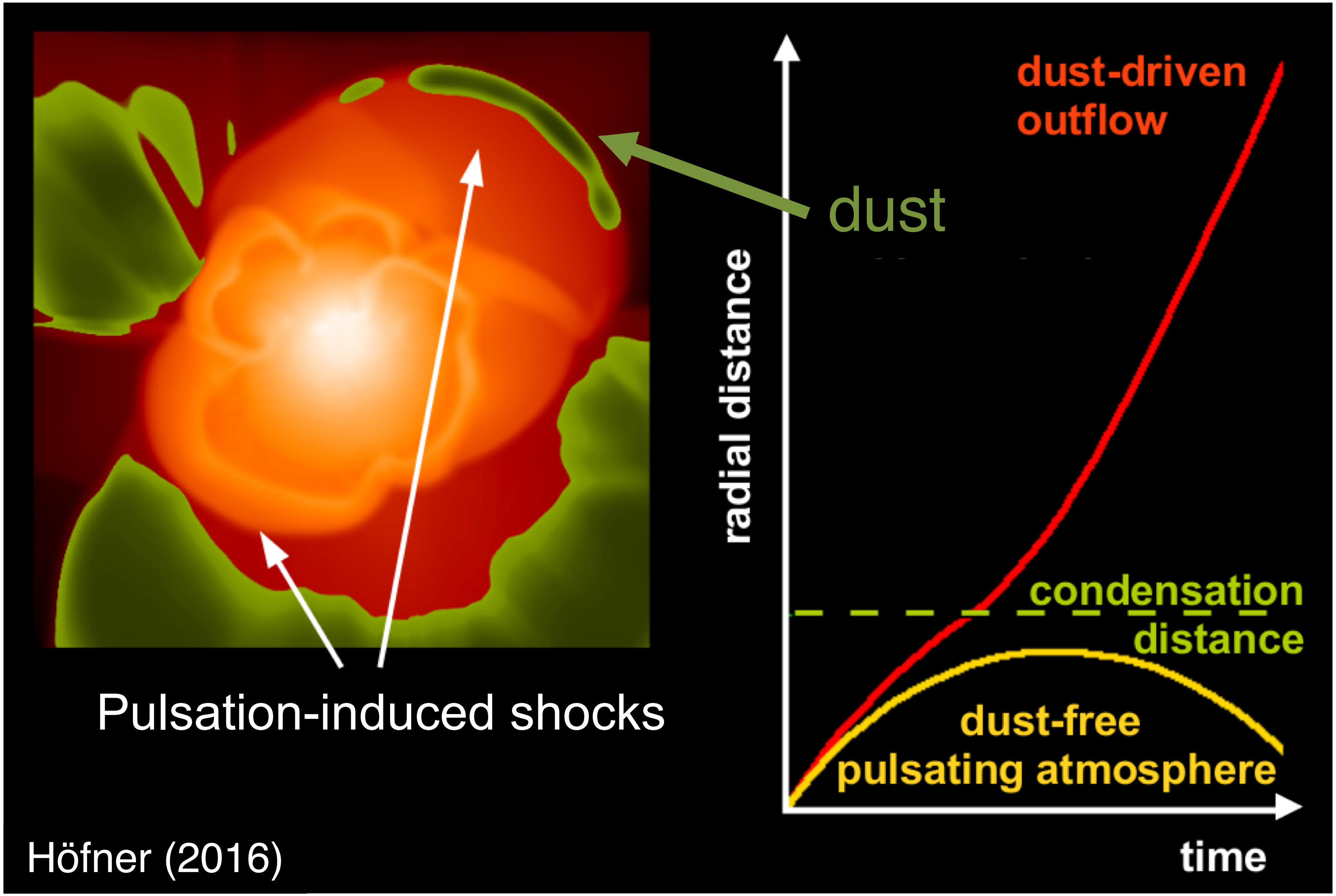

dust

Pulsation-induced shocks

Höfner (2016)

Wind acceleration

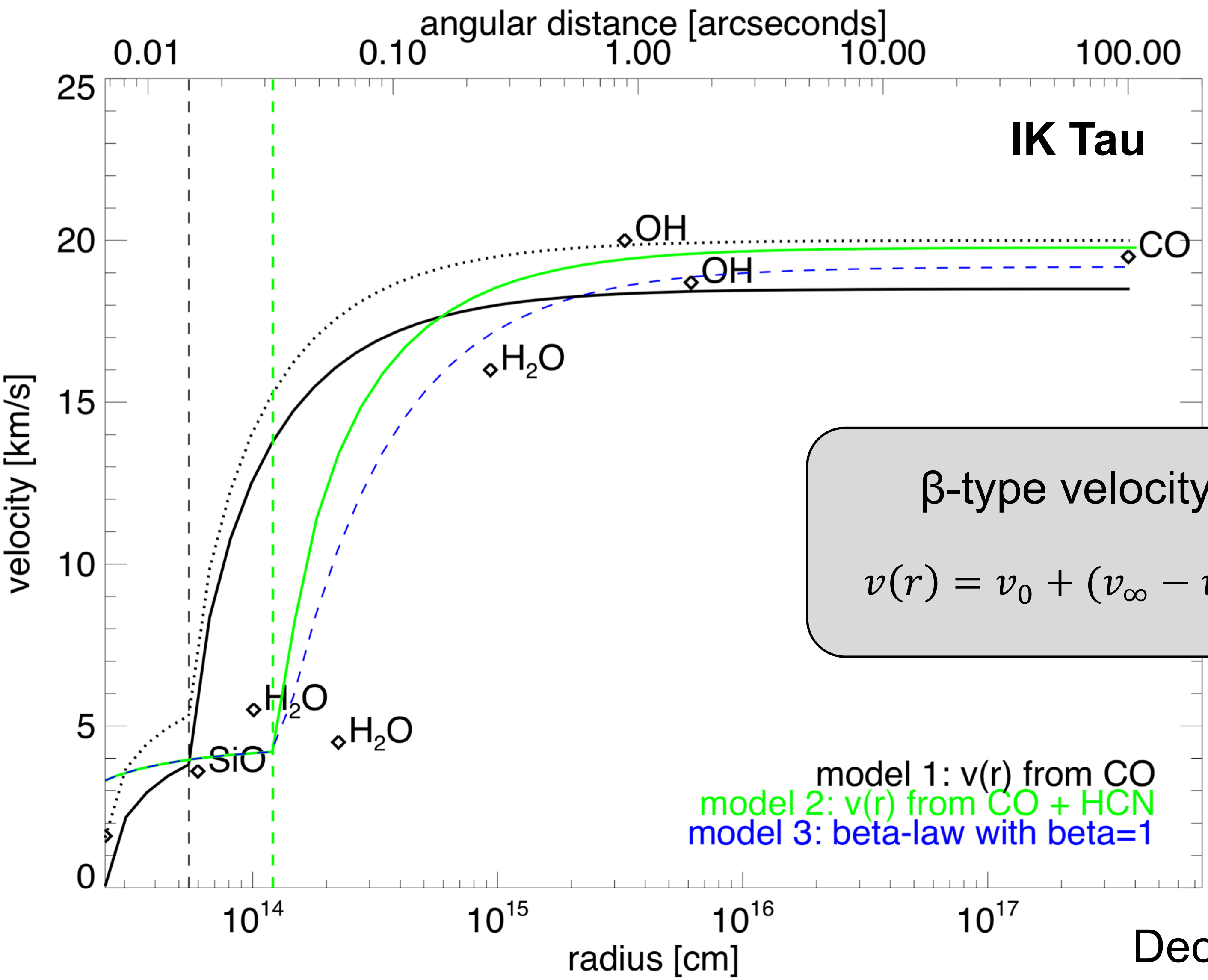

Terminal velocity

v_∞(CO)

β-type velocity profile

$$v(r) = v_0 + (v_\infty - v_0)\left(1 - \frac{r_0}{r}\right)^\beta$$

Decin et al. (2010)

Mass-loss rate and expansion velocity

$\dot{M}$

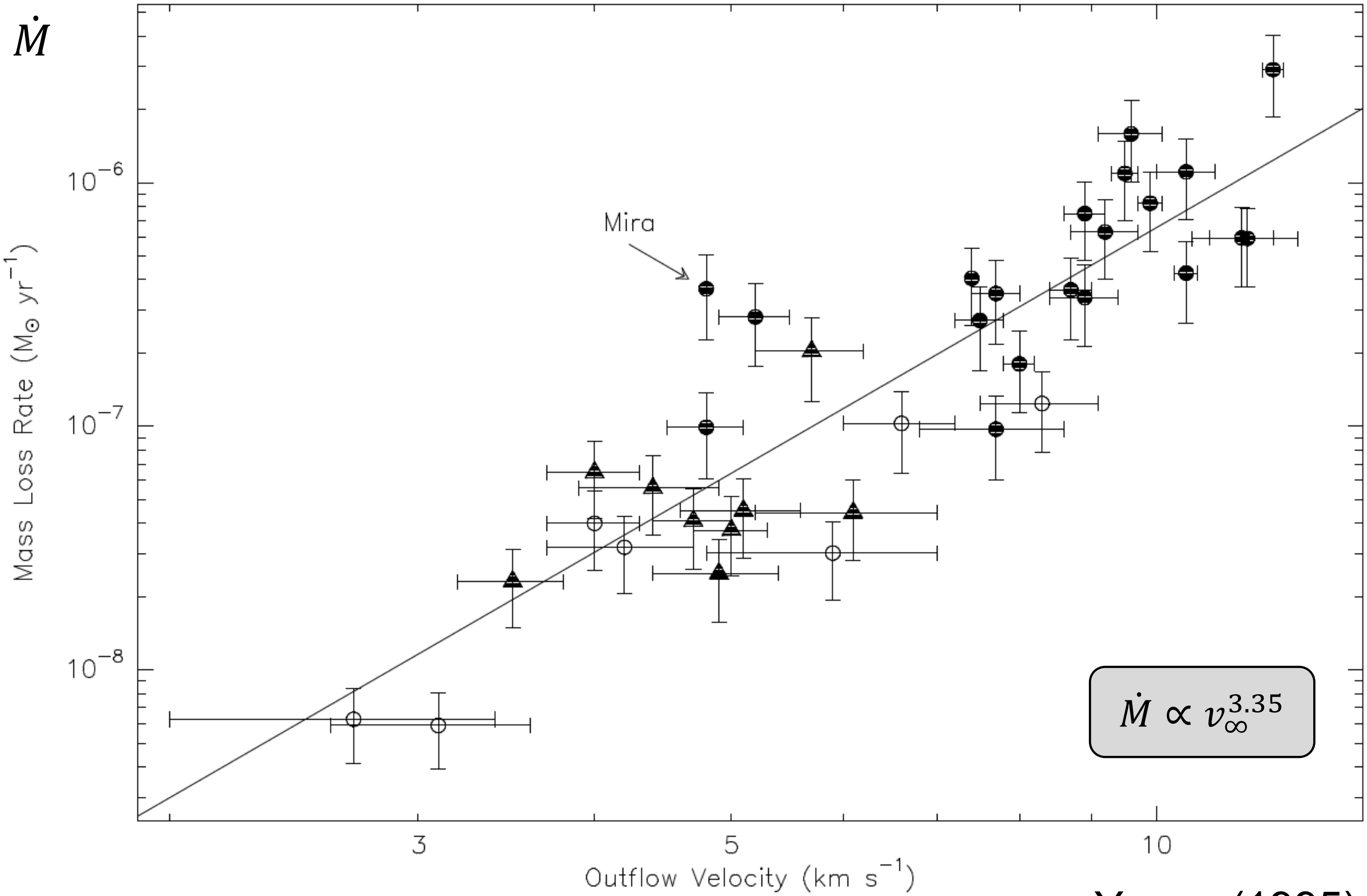

$\dot{M} \propto v_\infty^{3.35}$

Young (1995)

$v_\infty(\mathrm{CO})$

High-velocity SiO maser wings

- SiO v=1 J= 2–1 maser observations with the IRAM 30-m telescope
- v_∞(SiO) > v_∞(CO)
- SiO wing emission likely from the inner radii

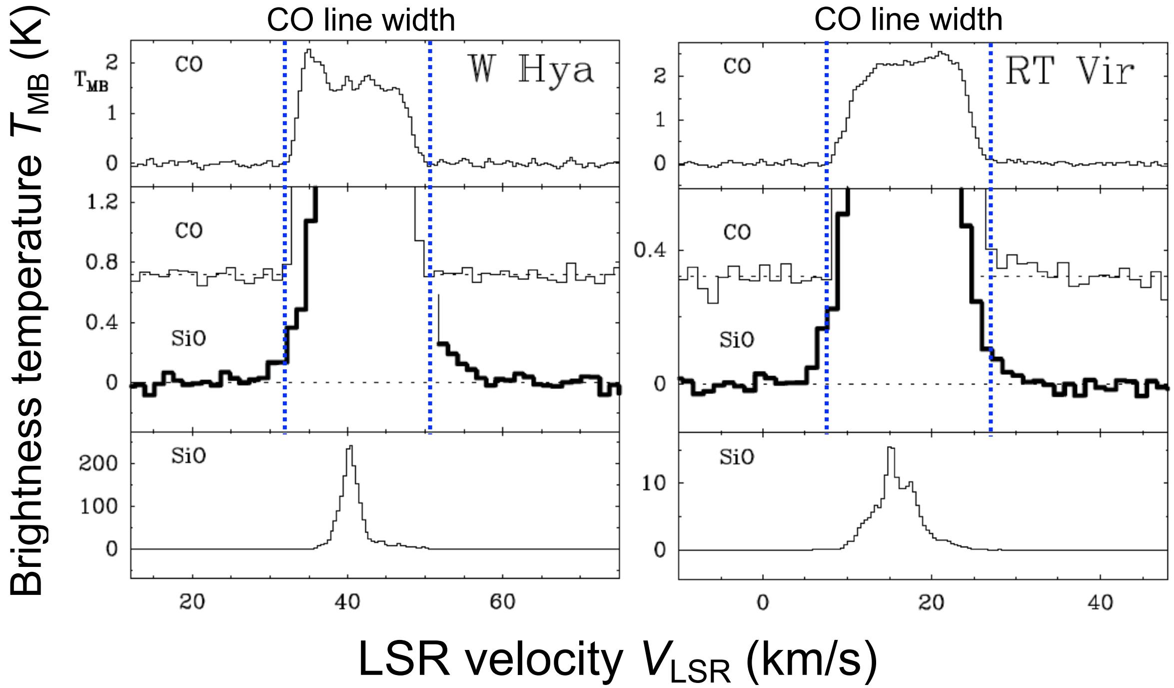

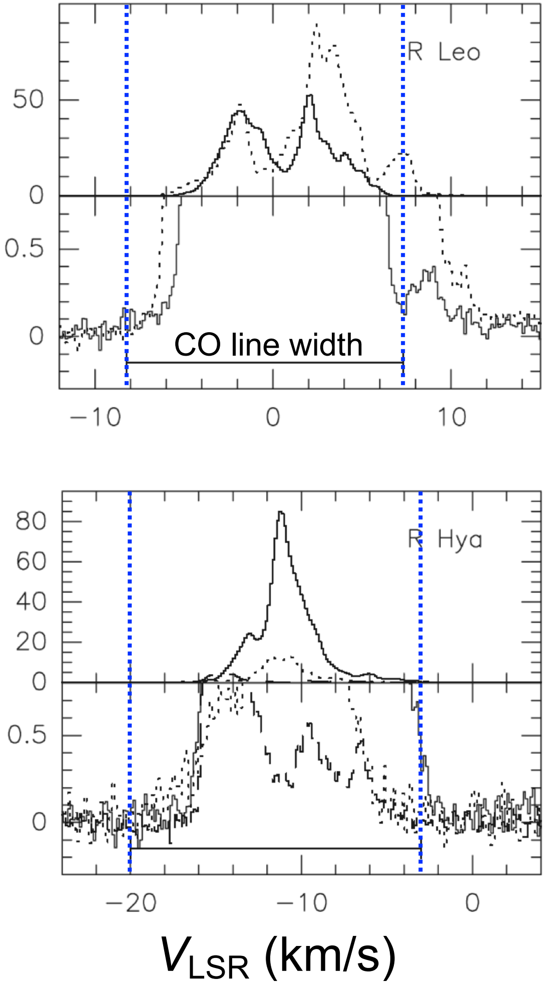

Cernicharo et al. (1997)

Herpin et al. (1998)

High-velocity SiO maser wings

- SiO v=1 J= 2–1 maser observations with the IRAM 30-m telescope
- v_∞(SiO) > v_∞(CO)
- SiO wing emission likely from the inner radii

Mass conservation

$$\dot{M}(r) = 4\pi r^2 \rho(r) v(r)$$

- H_2 gas densities derived from CO line observations
- $\dot{M}$ may be underestimated

Interferometric observations

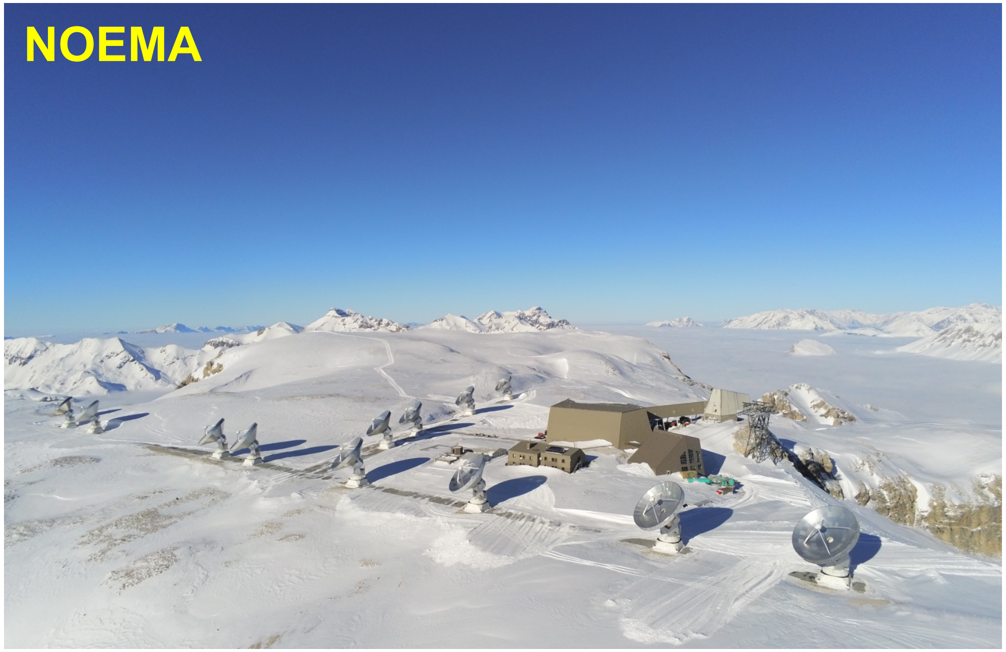

© IRAM, J. Boissier

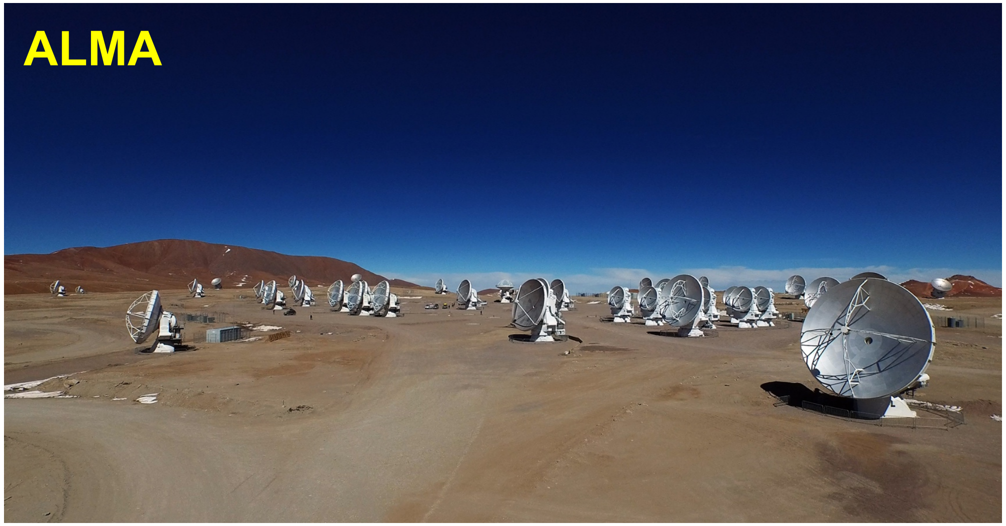

© L. Young

NOEMA capabilities

- 70.4–119.3 GHz / 127.0–182.9 GHz / 196.1–276.0 GHz
- Instantaneous bandwidth of ~31 GHz (7.744 GHz/sideband/pol.)
- New 250 kHz correlator mode
- New extended A configuration: baselines up to 1700 m
  - 12 antennas
  - 0.7 arcsec at 100 GHz / 0.3 arcsec at 230 GHz

© IRAM, F. Xavier Cuvelier

Larger line widths in new observations

RS Cnc (NOEMA)

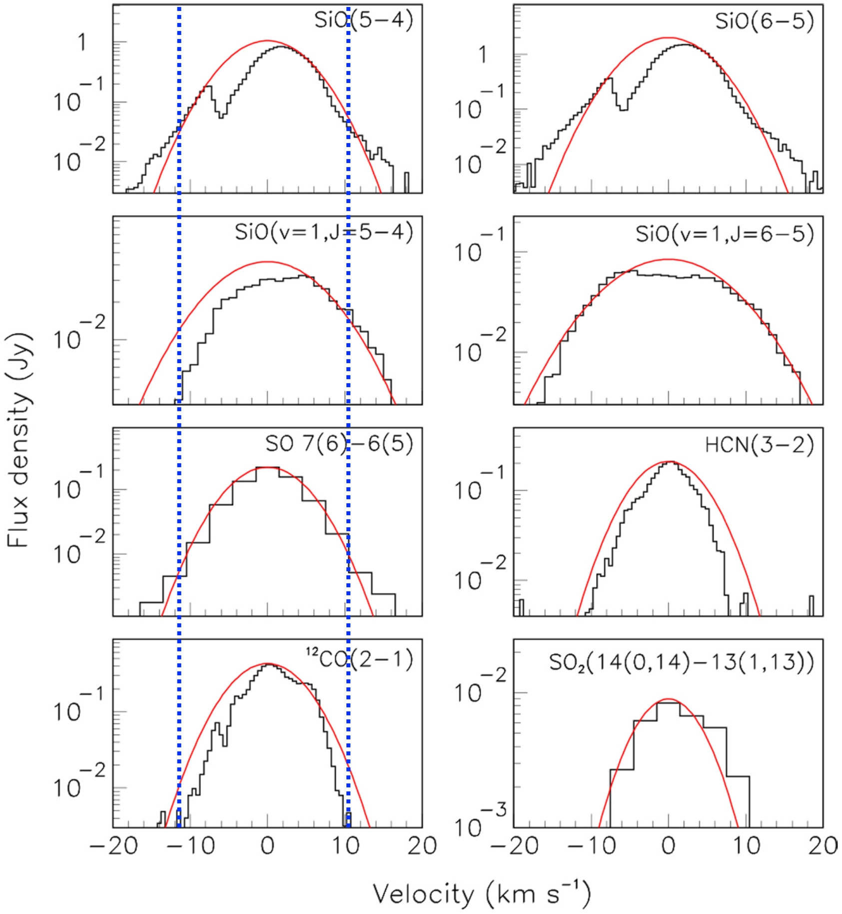

Winters et al. (2022)

IK Tau (ALMA)

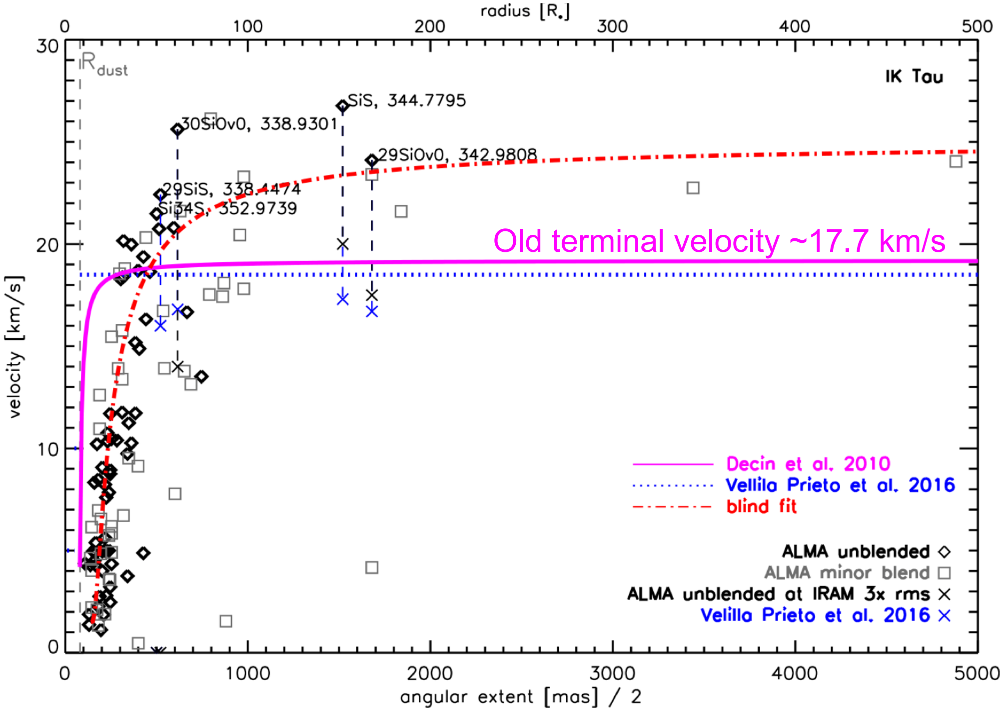

Old terminal velocity ~17.7 km/s

Decin et al. (2018)

Larger line widths in new observations

Mira (CSO, ALMA)

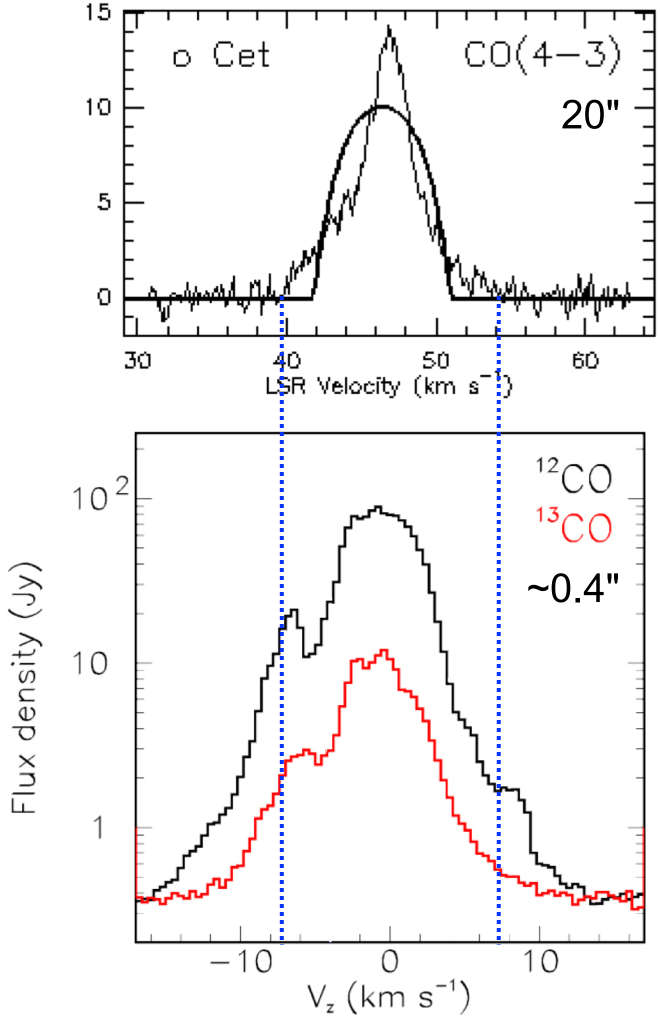

Young (1995); Nhung et al. (2022)

T Mic (ALMA)

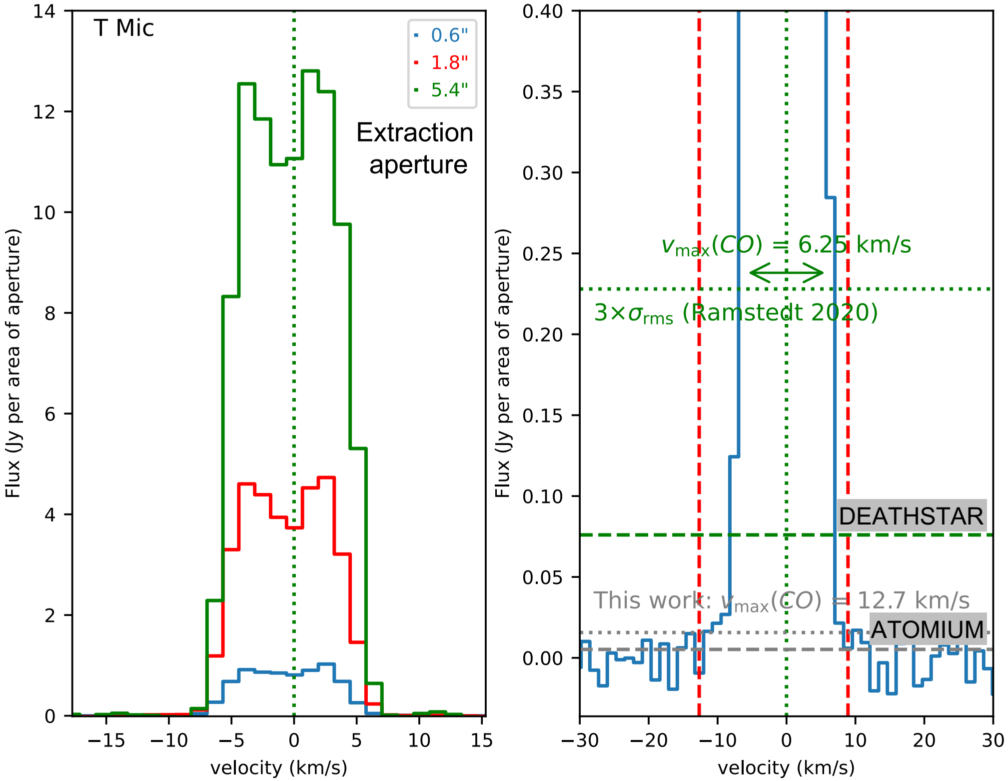

Ramstedt et al. (2020): Compact Array
Gottlieb et al. (2022): 12-m main array

ATOMIUM sample

- Higher v_∞(CO) with sensitive ALMA observations
- Higher v_∞ from other spectral lines (esp. SiO)

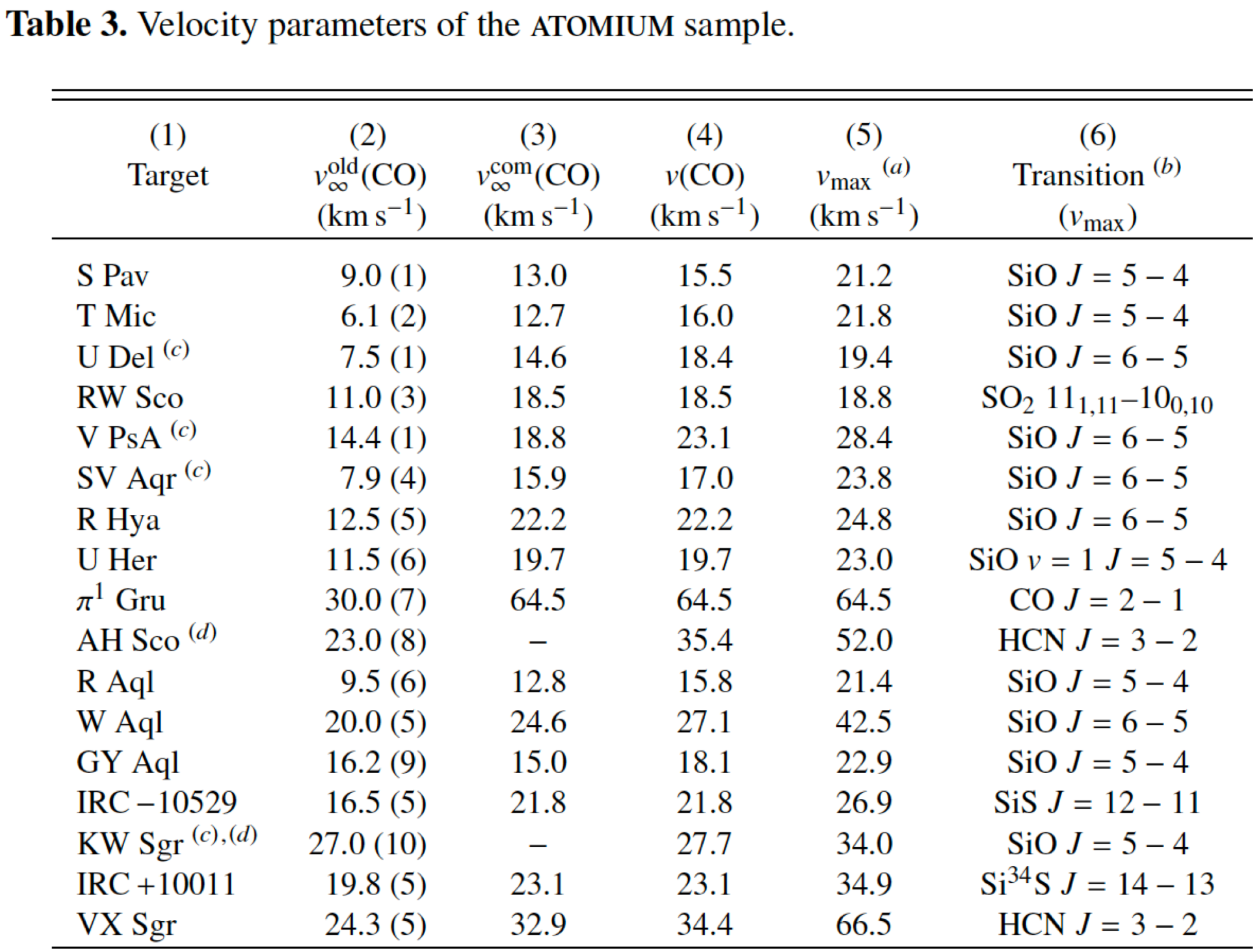

Table 3. Velocity parameters of the ATOMIUM sample.

(1) Target	(2) $v_\infty^{\rm old}$(CO) (km s^{-1})	(3) $v_\infty^{\rm com}$(CO) (km s^{-1})	(4) v(CO) (km s^{-1})	(5) $v_{\rm max}$ $^{(a)}$ (km s^{-1})	(6) Transition $^{(b)}$ ($v_{\rm max}$)
S Pav	9.0 (1)	13.0	15.5	21.2	SiO $J = 5 - 4$
T Mic	6.1 (2)	12.7	16.0	21.8	SiO $J = 5 - 4$
U Del $^{(c)}$	7.5 (1)	14.6	18.4	19.4	SiO $J = 6 - 5$
RW Sco	11.0 (3)	18.5	18.5	18.8	SO_2 $11_{1,11}-10_{0,10}$
V PsA $^{(c)}$	14.4 (1)	18.8	23.1	28.4	SiO $J = 6 - 5$
SV Aqr $^{(c)}$	7.9 (4)	15.9	17.0	23.8	SiO $J = 6 - 5$
R Hya	12.5 (5)	22.2	22.2	24.8	SiO $J = 6 - 5$
U Her	11.5 (6)	19.7	19.7	23.0	SiO $v = 1$ $J = 5 - 4$
π^1 Gru	30.0 (7)	64.5	64.5	64.5	CO $J = 2 - 1$
AH Sco $^{(d)}$	23.0 (8)	–	35.4	52.0	HCN $J = 3 - 2$
R Aql	9.5 (6)	12.8	15.8	21.4	SiO $J = 5 - 4$
W Aql	20.0 (5)	24.6	27.1	42.5	SiO $J = 6 - 5$
GY Aql	16.2 (9)	15.0	18.1	22.9	SiO $J = 5 - 4$
IRC −10529	16.5 (5)	21.8	21.8	26.9	SiS $J = 12 - 11$
KW Sgr $^{(c),(d)}$	27.0 (10)	–	27.7	34.0	SiO $J = 5 - 4$
IRC +10011	19.8 (5)	23.1	23.1	34.9	$Si^{34}S$ $J = 14 - 13$
VX Sgr	24.3 (5)	32.9	34.4	66.5	HCN $J = 3 - 2$

Gottlieb et al. (2022)

High-velocity line wings

- Thermal & turbulent line broadening (~1–2 km/s)
  - Insufficient to explain the broad line wings
- Pulsations
  - Redshifted (infalling) gas may appear in front of the stellar surface

↓ An example model from Höfner et al. (2016)

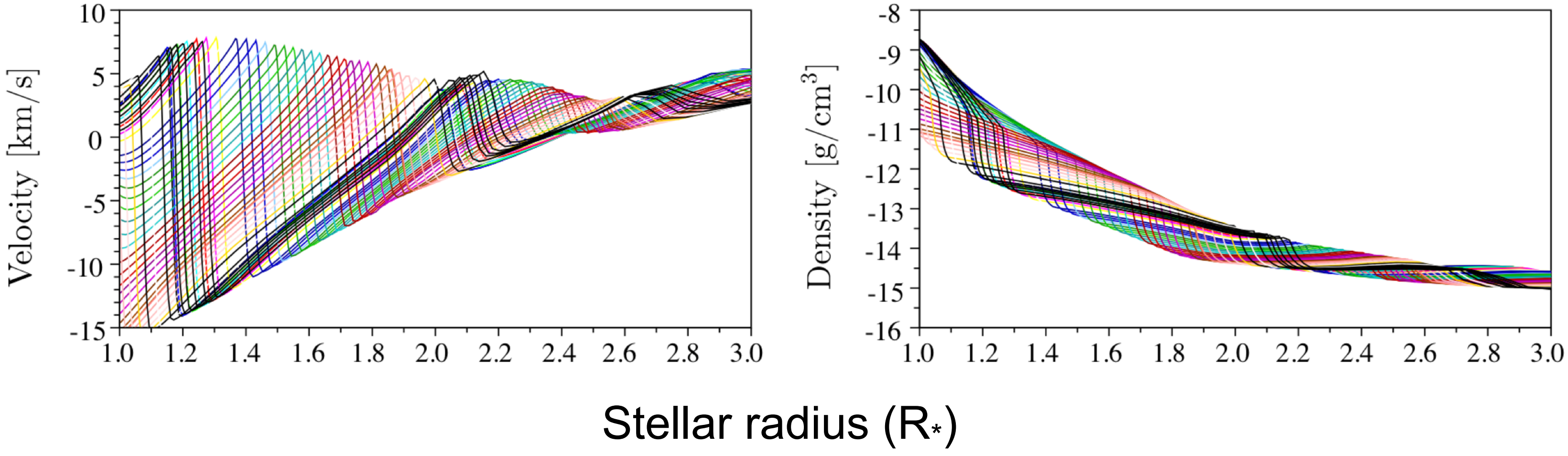

Pulsations

- Observationally confirmed with observations using the longest ALMA baselines (~16 km)

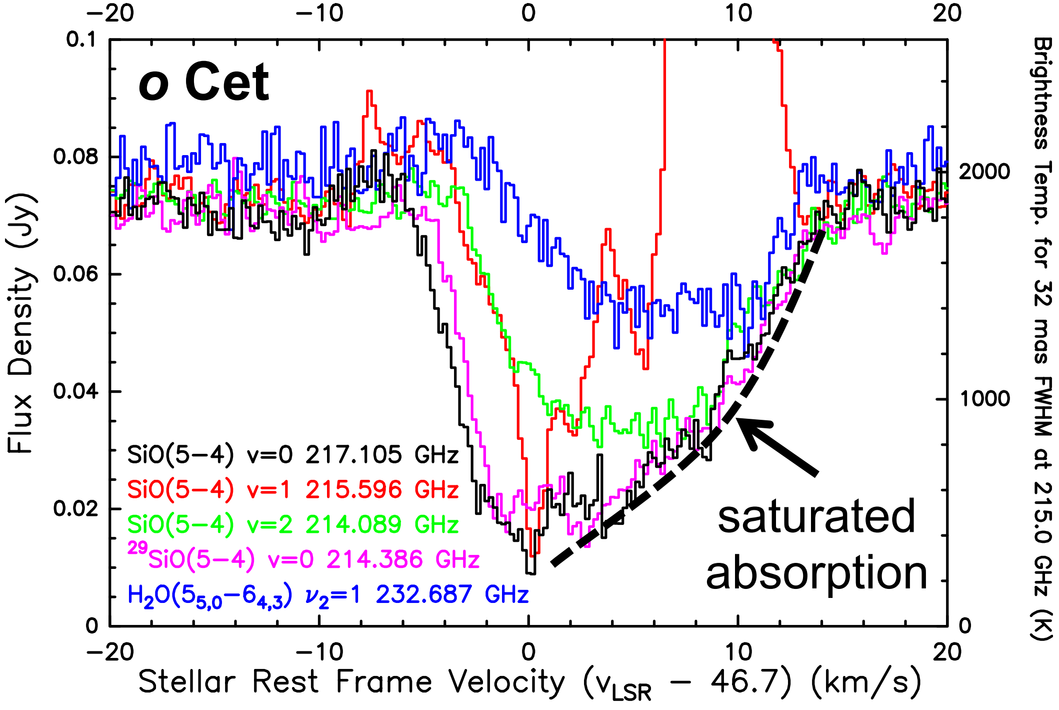

Wong et al. (2016)

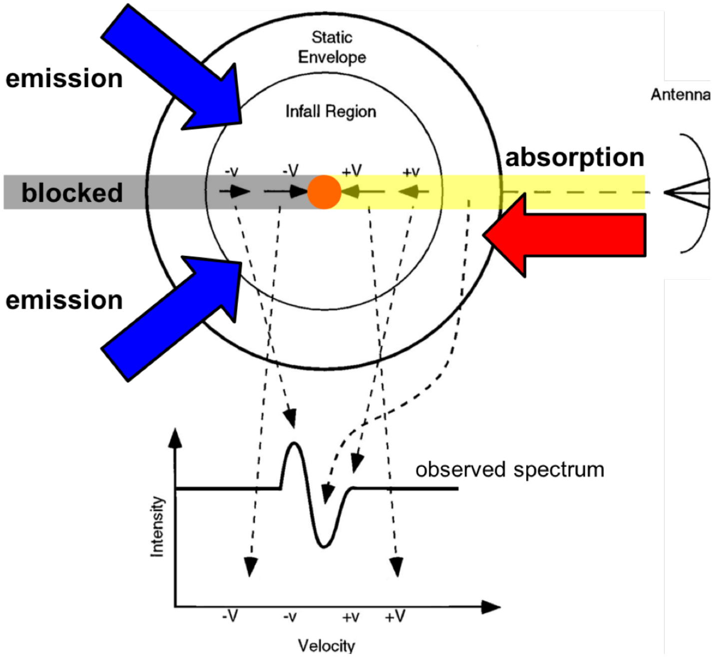

Adapted from Evans, N. J. II (1999)

Pulsations

- Observationally confirmed with observations using the longest ALMA baselines (~16 km)

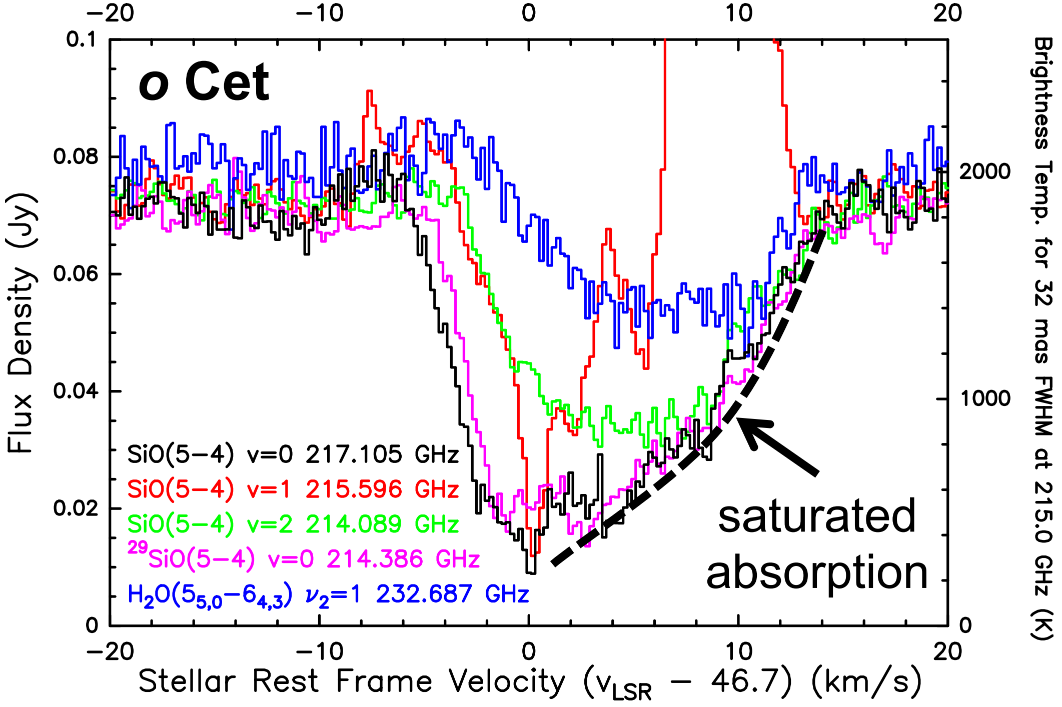

saturated absorption

Wong et al. (2016)

Velocity profile in radiative transfer model

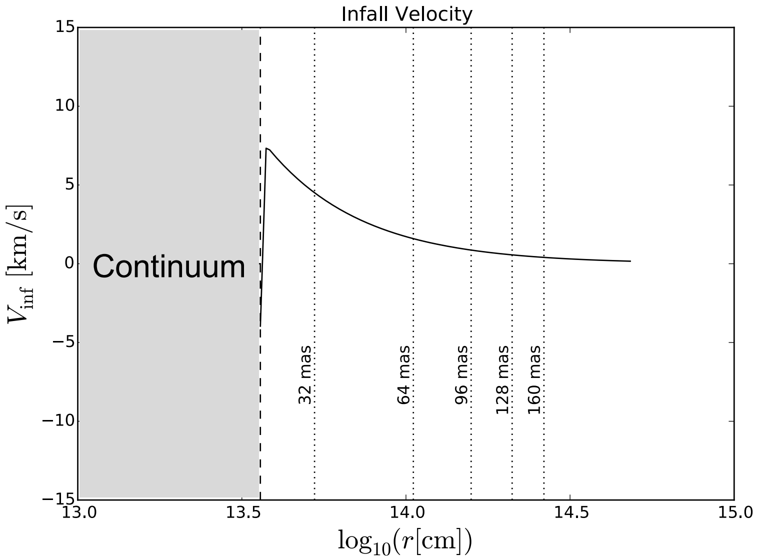

Pulsations

- Decin et al. (2018) estimated that the velocity variation due to pulsations was negligible due to relatively low energy levels of detected (sub)millimetre spectral lines.

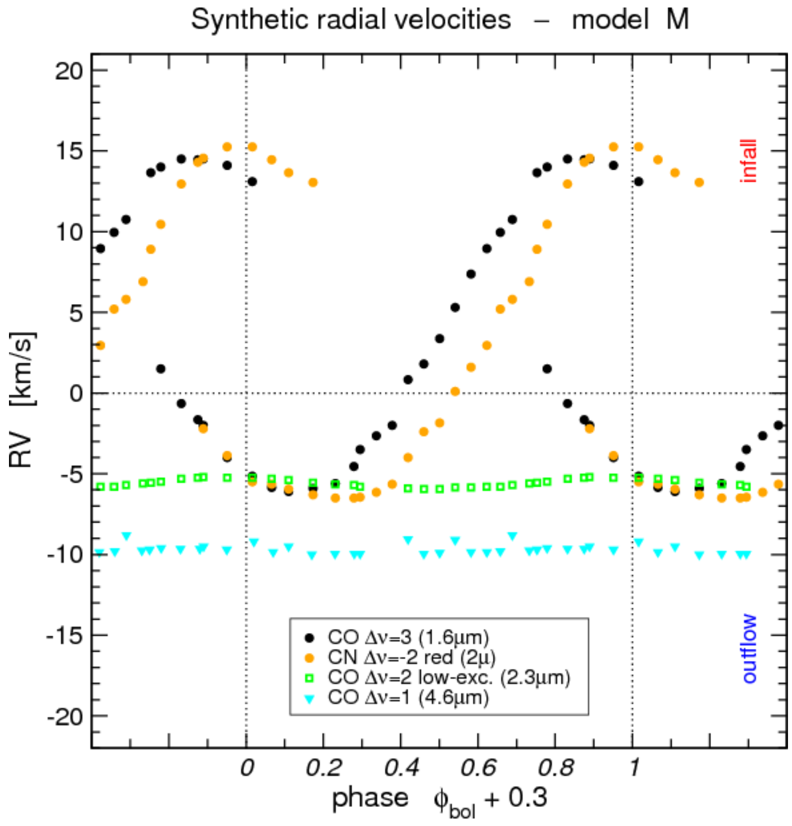

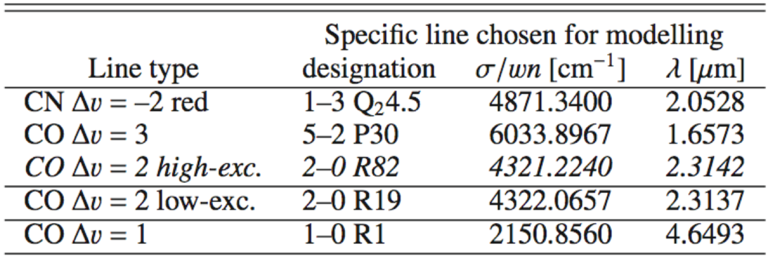

	Specific line chosen for modelling		
Line type	designation	σ/wn [cm^{-1}]	λ [μm]
CN $\Delta v = -2$ red	1–3 $Q_2$4.5	4871.3400	2.0528
CO $\Delta v = 3$	5–2 P30	6033.8967	1.6573
CO $\Delta v = 2$ high-exc.	*2–0 R82*	*4321.2240*	*2.3142*
CO $\Delta v = 2$ low-exc.	2–0 R19	4322.0657	2.3137
CO $\Delta v = 1$	1–0 R1	2150.8560	4.6493

Nowotny et al. (2010)

Pulsations

CO v=1 J= 2–1 in R Hya →

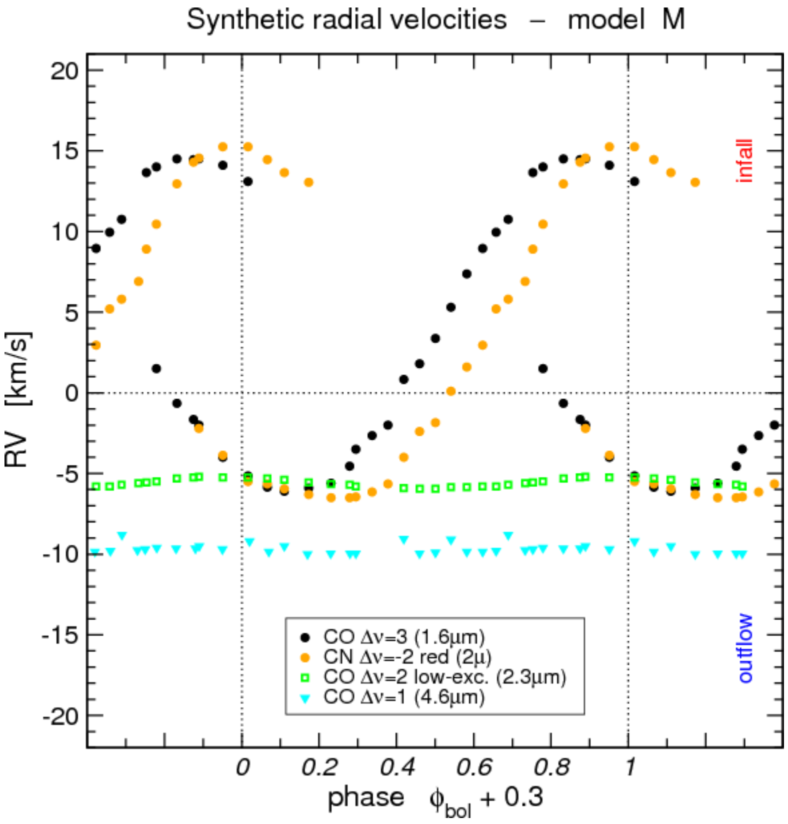

Nowotny et al. (2010)

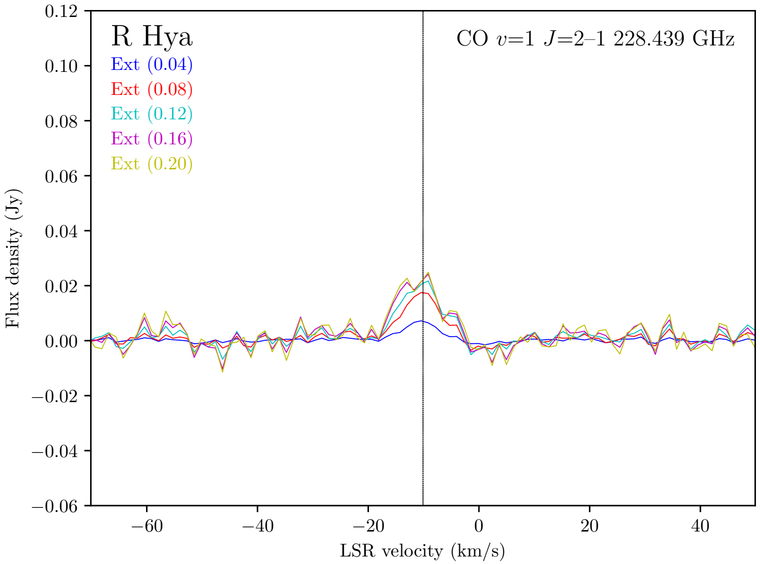

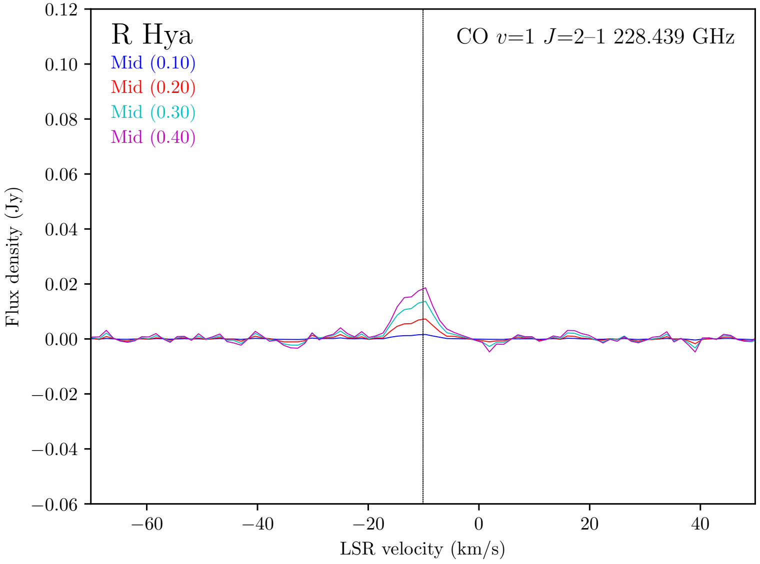

Pulsations

- Gottlieb et al. (2022) found that pulsation-driven shocks cannot explain the observed velocity measures in their radiative transfer models.

Velocity profile adapted from Bladh et al. (2019)

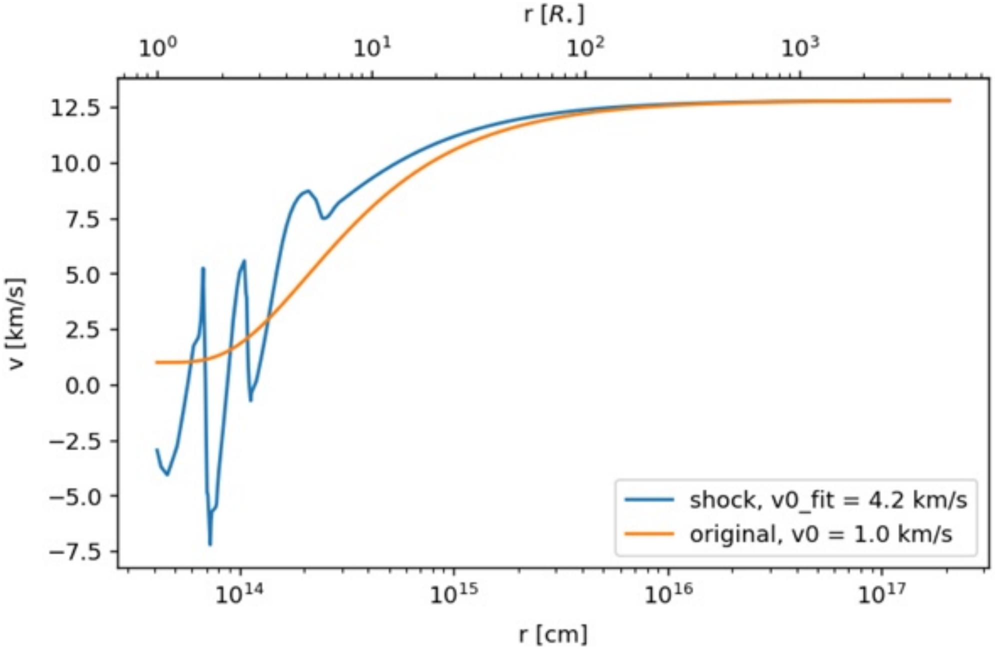

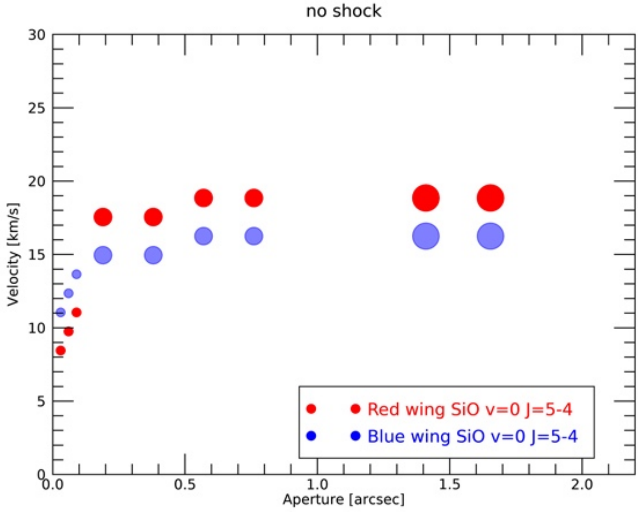

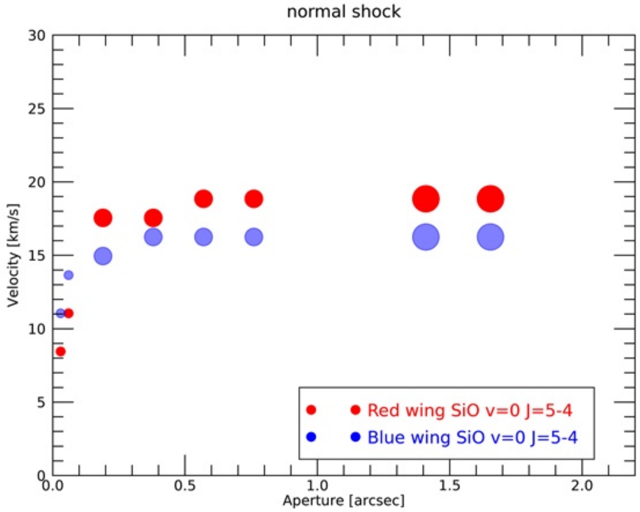

Binary interactions

- Decin et al. (2020) argued that interaction with (sub)stellar companion can be the dominant wind-shaping mechanism for most observed AGB stars.

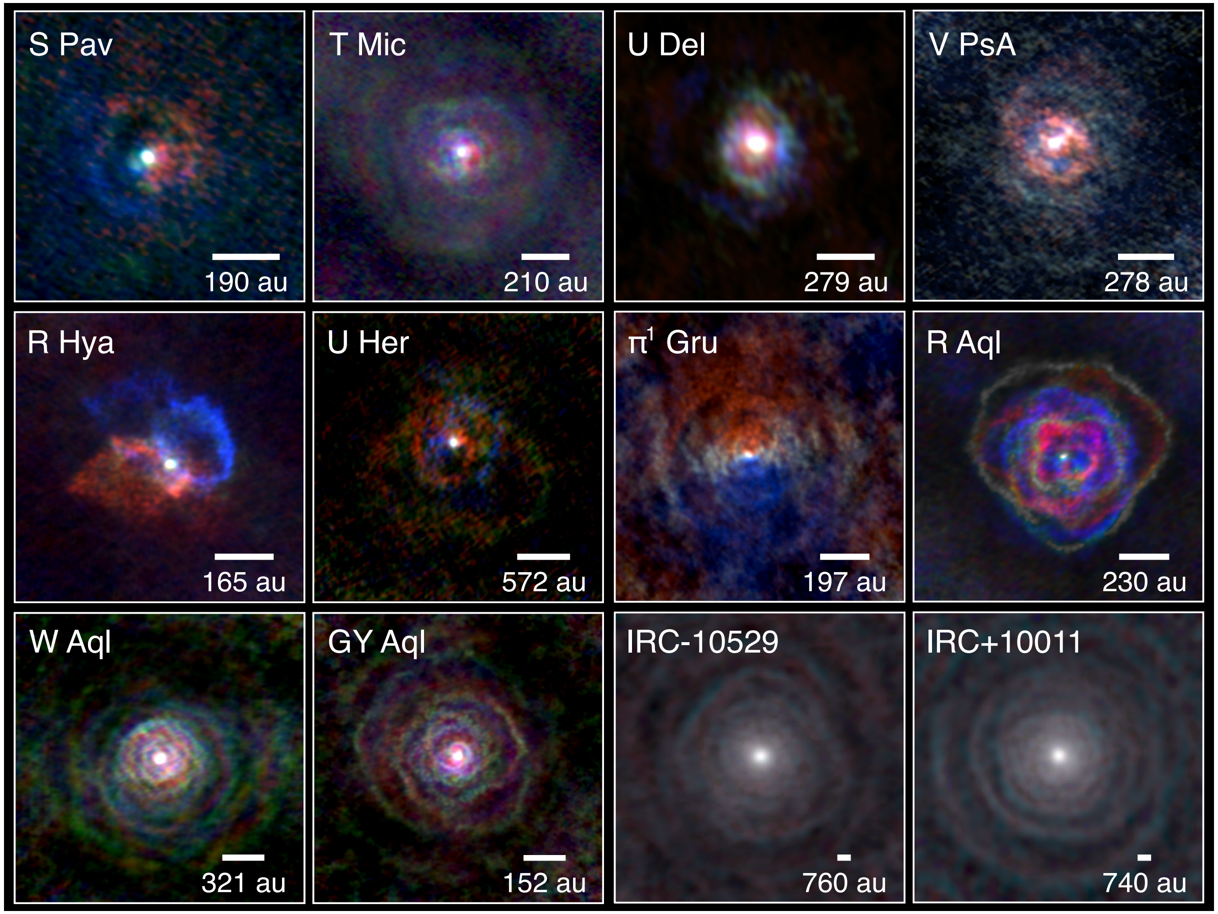

Binary interactions

- Gottlieb et al. (2022) suggest that binary interaction may also produce non-monotonic velocity structures.

↓ 3D hydrodynamical simulation by El Mellah et al. (2020)

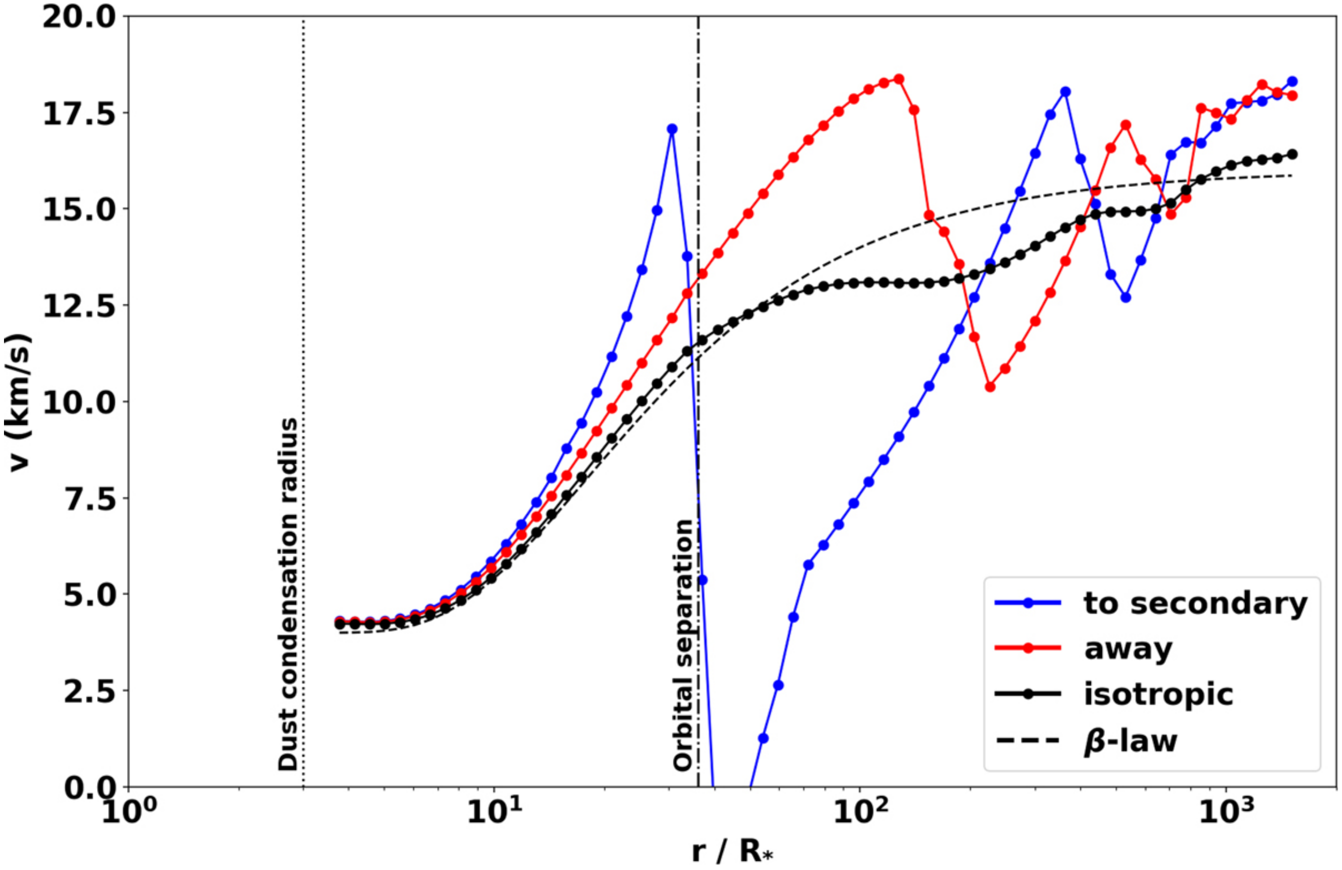

Binary interactions

- Gottlieb et al. (2022) suggest that binary interaction may also produce non-monotonic velocity structures.
  - Preferential direction of outflows
  - Equatorial density enhancement (EDE) may occur with a density contrast of up to an order of magnitude
  - Dust mass-loss rates based on spherical symmetry may be systematically overestimated

The case of R Hya

- Significant non-zero offsets of high-velocity SiO emission in position-velocity (PV) diagrams (Homan et al. 2021)
  - ➢ High-v components do not come from the atmosphere
  - ➢ Possibly a differentially rotating disc

CO SiO SiO

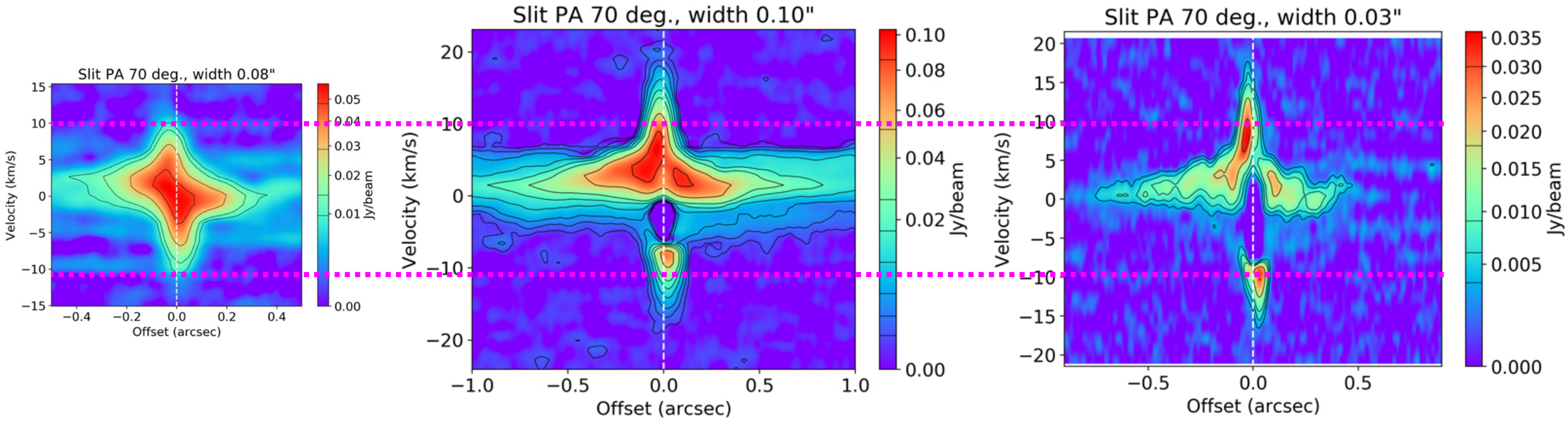

Homan et al. (2021)

The case of R Hya

- Shocks induced by pulsations and convective cell ejections are suggested by Nhung et al. instead.

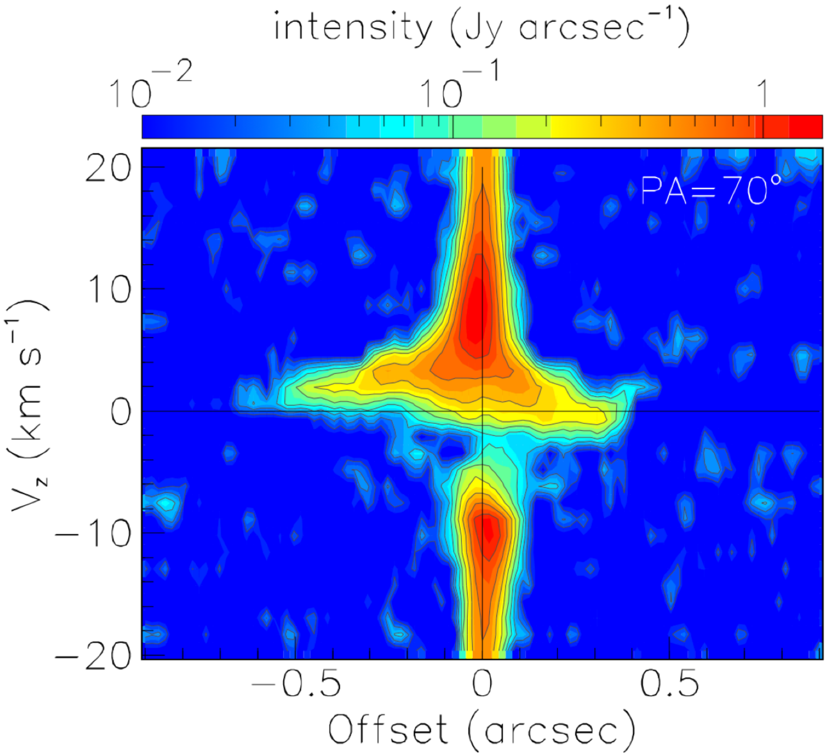

Nhung et al. (arXiv:2207.06690)
Without continuum subtraction

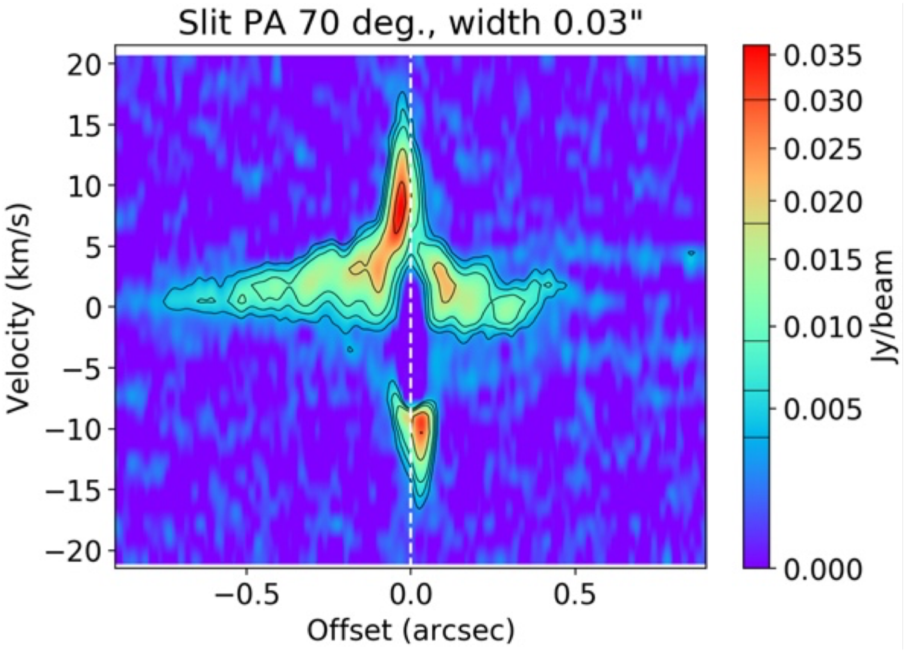

Homan et al. (2021)
Continuum-subtracted

Summary

- High-velocity wings exceeding the terminal velocity derived from CO line profiles are seen in multiple O-rich AGB stars.
- High-angular-resolution and sensitive ALMA observations reveal broad and low-level CO emission line wings.
- Various molecular transitions trace high-velocity features (e.g. SiO, H_2O, SiS, HCN).
- Possible causes include pulsation-induced shocks, binary interaction of a close companion, rotation.
- Detailed analyses and radiative transfer modelling of individual objects will be necessary.